Process-scale modelling of microstructure in direct chill casting of aluminium alloys

M Bedel, L Heyvaert, M Založnik, H Combeau, D Daloz and G Lesoult
Institut Jean Lamour, CNRS – Université de Lorraine, F-54011 Nancy CEDEX, France

E-mail: marie.bedel@univ-lorraine.fr

Abstract. The mechanical properties of an alloy being related to its microstructure, the understanding of the mechanisms responsible for the grain structure formation in direct chill casting is crucial. However, the grain size prediction by modelling is difficult since a variety of multi-scale coupled phenomena have to be considered. Nucleation and growth of the grains are interrelated, and the macroscopic transport phenomena such as the motion of grains and inoculant particles with the flow impact the nucleation-gowth competition. Thus we propose to study the grain size distribution of a 5182 alloy industrial scale slab of 510 mm thickness, both non-inoculated and inoculated with Al-3Ti-1B, for which experimental grain size measurements are available. We use a volume-averaged two-phase multi-scale model that describes nucleation from inoculant particles and grain growth, fully coupled with macroscopic transport phenomena: fluid flow induced by natural convection and solidification shrinkage, heat, mass and solute mass transport, grains and inoculant particles motion. We analyze the effect of liquid and grain motion as the effect of grain morphology on microstructure formation and we show in which extent those phenomena are responsible for the grain size distribution observed experimentally. The effect of the refiner level is also studied.

1. Introduction

Grain refiners are commonly used in DC casting of aluminium alloys in order to refine the microstructure. Not only the average grain size is reduced but the size distribution is homogenized [1][2]. When refiners are added in the melt, nucleation, i.e. grain initiation, is supposed to be athermal and heterogeneous. Grains form on inoculant particles instantaneously as soon as a critical undercooling, which depends on their size, is reached. The size distribution of inoculant particles was determined for industrially used refiners such as Al-Ti-C and Al-Ti-B [3]. Coupled with a growth model, it enabled to predict the competition between nucleation and growth of grains at the microscopic scale and thus the final grain size when using these refiners [4]. Indeed, the heat release induced by grain growth tends to reduce the local undercooling and thus to prevent the activation of further inoculant particles. This type of model can explain the decrease of the grain size with an increase of the cooling rate due to the competition between nucleation and growth. But what happens in macroscopic systems, where convection phenomena cannot be neglected anymore?

In most of the macroscopic solidification models, grains are supposed to nucleate instantaneously at a unique temperature. Moreover, the transport of grains is either strongly simplified or neglected [5][6]. The transport of inoculant particles has never been considered to our best knowledge. This can explain why only few models propose a comparison with experiments in terms of grain size

Content from this work may be used under the terms of the Creative Commons Attribution 3.0 licence. Any further distribution of this work must maintain attribution to the author(s) and the title of the work, journal citation and DOI.
Published under licence by IOP Publishing Ltd

distribution. We can name the work of Håkonsen et al., where different nucleation laws were tested [7] but where both the motion of inoculant particles and equiaxed grains were neglected. Indeed, these transport phenomena impact the local competition between nucleation and growth of grains and thus the final grain size distribution.

Moreover, the inoculant particles and grains transport can alter the grain morphology locally. In a closed system, when the melt is rich in inoculant particles, the resulting grain density is high enough to result in a globular grain morphology. This hypothesis is made in most of macroscopic solidification models. However, when grains and inoculant particles are free to move, they can leave the nucleation area and thus their growth and their morphology is strongly affected by their motion. Thus in our work, we propose to study the impact of combined transport phenomena on the final grain size distribution, taking into account their morphology.

2. Model description

The description of the volume-averaged two-phase multiscale model we use is given in [8], so we only present its main features and the extensions which were made since. At the macroscopic scale, the model accounts for heat, mass, solute mass, grains and inoculant particles transport coupled with flow driven by natural convection (modelled through the Boussinesq assumption) and solidification shrinkage (supposed to be constant). Two flow regimes are distinguished: when the grain fraction (which is different from the solid fraction when grains are dendritic) is locally larger than the imposed packing limit g_{pack}, the grains are supposed to be blocked and to move at the casting velocity while the liquid flow through the porous solid matrix is modelled considering the drag interactions by a Darcy term. When the grain fraction is smaller than g_{pack}, the solid phase transport is modelled through a solid viscosity in a pseudo fluid model [9]. In this way, the solid phase inertia and internal stress are taken into account.

Nucleation is supposed to be athermal and heterogeneous, which means that a grain forms instantaneously on an inoculant particle of diameter d when the undercooling reaches a critical value ($\Delta T(d)=4\Gamma/d$, where Γ is the Gibbs-Thomson coefficient). The inoculant-particle size distribution is approximated in this work by an exponential law: $N(d)=N_0/d_0\exp(-d/d_0)$, whose parameters are estimated in [3] for the Al-5Ti-1B refiner (as no such parameters are known for the Al-3Ti-1B refiner). At the macroscopic scale, the inoculant particles are supposed to be transported with the liquid, which is modelled by solving separately the transport equation of several inoculant particles classes. To do so, the size distribution law is discretized into classes, as shown in Figure 1.

Phase change is supposed to be controlled by solute diffusion in both liquid and solid phases at the grain scale. Local thermal equilibrium and thermodynamic equilibrium are supposed at the solid-liquid interface and analytical expressions are used for diffusion lengths [10][11]. When not stated otherwise, the growing solid structures are assumed to have a spherical shape, which can correspond to globular grains, but a dendritic model has been also developed. Indeed, the transport and the packing of the grains depend on their morphology. Moreover, the grain morphology impacts the growth kinetics and thus the competition between nucleation and growth of the grains. We suppose that the grains envelopes are octahedrons and the tips are considered to be paraboloidal [12].

3. Experimental results and case modeling

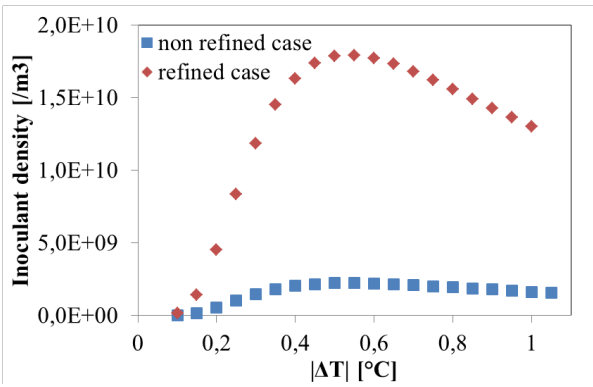

Figure 1. Inoculant classes corresponding to 1 kg/t of Al-5Ti-1B refiner in red and to 0.125 kg/t of Al-5Ti-1B refiner in red [3].

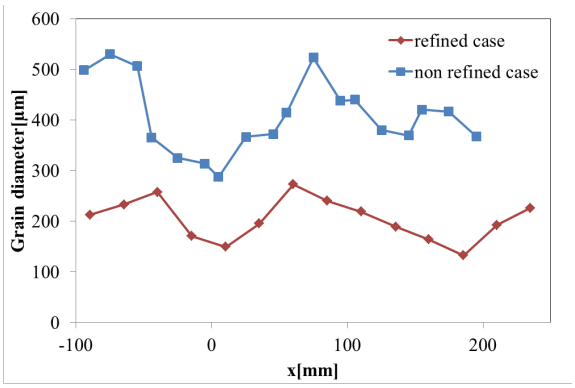

Figure 2. Experimental profile of final grain diameter, as a function of ingot thickness for the refined case in red and for the non-refined case in blue [2].

We modeled the solidification of a 5182 alloy industrial scale slab of 510 mm thickness and 1897 mm width, solidified at v_c= 1mm/s, without refinement and then with the addition of 1 kg/t of Al-3Ti-1B, casted in the frame of the BRITE EURAM project EMPACT [2] [13] [14]. Image analysis on optical microscopy images from samples taken along the ingot thickness enabled to obtain the average grain diameter profile for the non-refined and for the refined cases, as shown in Figure 2 [14].

Table 1. Thermo-physical data of Al-4.06wt.%Mg [5].

Property	Unit	Value
Density	kg m^{-3}	2 400.0
Specific heat	J kg^{-1} K^{-1}	1 107.0
Thermal conductivity, solid	W m^{-1} K^{-1}	109.0
Thermal conductivity, liquid	W m^{-1} K^{-1}	100.0
Diffusion coefficient, solid	m^2 s^{-1}	1.8 x 10^{-12}
Diffusion coefficient, liquid	m^2 s^{-1}	7.7 x 10^{-9}
Latent heat of pure Al	J kg^{-1}	3.725 x 10^5
Liquid dynamic viscosity	Pa s	1.2 x 10^{-3}
Thermal expansion coefficient	K^{-1}	1.245 x 10^{-4}
Solutal expansion coefficient	wt.$\%^{-1}$	4.0 x 10^{-3}
Pure Al melting temperature	°C	660.5
Eutectic temperature	°C	450.0
Liquidus slope	°C wt.$\%^{-1}$	-5.831
Partition coefficient	-	0.485
Gibbs-Thomson coefficient	K.m	1.9x10^{-7}

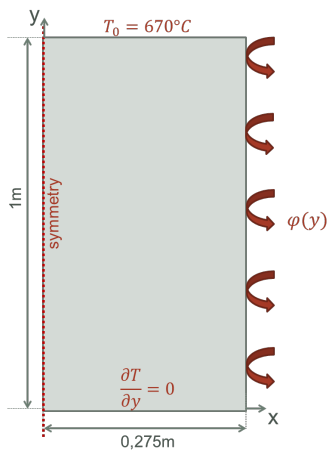

Figure 3. Model geometry and boundary conditions.

We model the 5182 alloy by a Al-4.06wt.%Mg alloy, whose thermo-physical properties are given in Table 1 [5]. The refiner size distribution for 1 kg/t of Al-5Ti-1B is taken from [3] and is discretized by considering constant undercooling intervals as shown in Figure 1. The non-refined part of the ingot is modeled by considering a modified refiner size distribution, as the nucleation is considered to occur only in refiner particles in the model. According to the experimental grain size profiles (Figure 2), the average grain size is almost doubled when the refiner is suppressed, which corresponds to a grain density divided by 8. Thus we use the same refiner size distribution for the non-refined case but for 0.125 kg/t addition of Al-5Ti-1B (Figure 1).

The ingot width being much larger than its thickness, we consider a two-dimensional system 1m high (y axis) and 275 mm thick (x axis) as represented in Figure 3. By assuming an axial symmetry in x=0, we have to model only half of the ingot thickness. Although the melt is injected through a combo-bag in the experiment, we suppose that the melt is injected through the whole ingot thickness. The entry temperature of the melt is T_0=670°, as measured by a thermocouple at the melt surface. The surface heat extraction rate $\phi(y)$ has been determined by an inverse method as a function of the height [15].

Table 2. hypotheses made for the case modeling (v_p: velocity of the product, v_l: liquid velocity).

	Liquid motion	Inoculant particle velocity	Grain motion	Dendritic morphology	Nucleation law
Case 0	No	v_p	No	No	Refined case
Case 1	Yes	v_l	No	No	Refined case
Case 2	Yes	v_l	Yes	No	Refined case
Case 3	Yes	v_l	Yes	Yes	Refined case
Case 4	Yes	v_l	Yes	Yes	Non-refined case

All the calculations are made with a time step $\Delta t=10^{-3}$s and a regular mesh composed of 51x200 square cells. In order to study the impact of macroscopic transport phenomena and grains morphology on the microstructure prediction, we study 5 cases of increasing complexity. In Case 0, no convective transport phenomenon is considered. In Case 1, liquid motion is taken into account through natural convection and solidification shrinkage and the inoculant particles are transported with the liquid phase. Then in Case 2, the grain motion is added and the packing grain fraction is fixed to g_{pack}=0.3. In Case 3, we add the effect of grain morphology by considering a paraboloidal tip shape for calculating the tip velocity of the stems of the grains. Finally, in Case 4, the model hypotheses are kept identical, but the nucleation law is changed in order to better fit the non-refined case.

4. Results and discussion

4.1. Impact of liquid motion

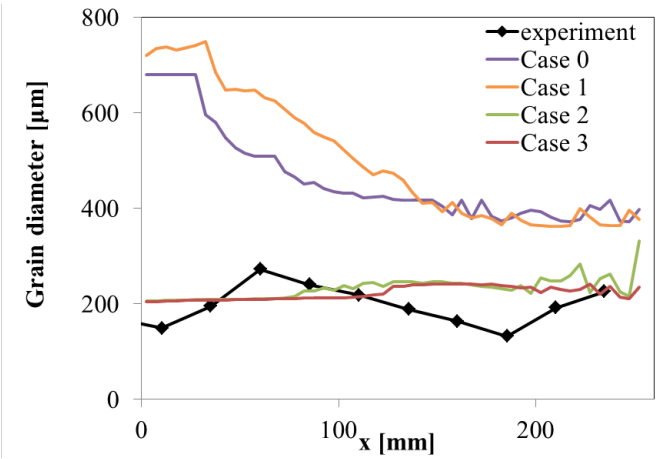

Figure 4. Grain diameter profile obtained for Case 0 to Case 3, compared to the experiment.

Even when all the convective transport phenomena are neglected, the grain size prediction is not uniform in the ingot. We can see this for Case 0 in the grain diameter profile given in Figure 4. Indeed, the heat being extracted from the ingot sides, the cooling rate and thus the undercooling are larger closer to the ingot surface. This can be seen in Figure 5-a, which shows the profile of the maximal undercooling. Thus due to the higher undercooling close to the surface, more inoculant classes can be activated and the nucleation rate is larger (Figure 5-b), which explains the smaller grain size in this

region. Indeed, Figure 5-b shows the nucleation rate along the ingot thickness, which corresponds to the integral of the nucleation events per second at a given thickness in the ingot.

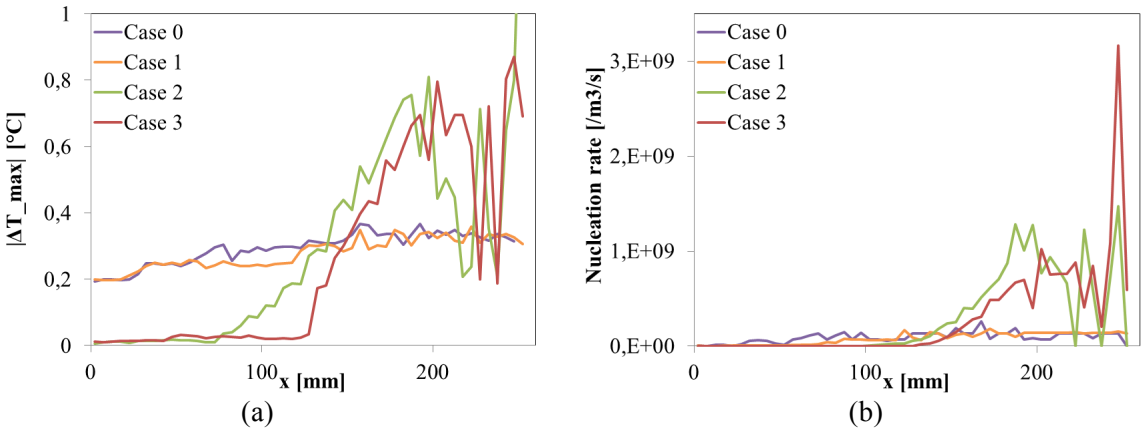

Figure 5. (a) maximal undercooling and (b) nucleation rate profiles, for Case 0 to Case 3.

When the liquid motion induced by natural convection and solidification shrinkage is added (Case 1), a clockwise flow loop appears. The cooling of the liquid close to the surface (which tends to induce a clockwise loop) more than compensates the liquid enrichment in solute induced by solidification (which would tend to reverse the flow direction). Thus the liquid cooled close to the surface is carried towards the centre of the ingot, favouring a uniform temperature distribution in the centre. However, the maximal undercooling is only slightly modified compared to Case 0 (Figure 5-a), but the final grain size tends to increase in the centre of the ingot (Figure 4). Indeed, as the inoculant particles are considered to move with the liquid, they pass by the ingot surface before reaching the centre. The inoculant particles classes activated close to the surface do not reach the centre and the competition between nucleation and growth is altered: fewer big particles reach the centre of the ingot, and with an identical maximal undercooling, fewer grains are formed. Thus we observe that the liquid and most of all the inoculant particles motion tends to amplify the grain size heterogeneities. However, the grain diameter profile is still far from fitting the experimental profile (Figure 4-a).

4.2. Impact of solid motion

When the effect of grain motion is taken into account (Case 2), we notice that the predicted grain size profile is strongly modified and is much closer to the experimental observations (Figure 4). The grain motion impacts the microstructure formation through two phenomena:

- Firstly, the grain motion in itself induces a redistribution of the grains in the ingot. In the studied case, grains are heavier than the liquid, therefore they settle in the centre of the ingot. Thus the grain motion tends to counter the thermal effect by increasing the grain density in the ingot centre.
- Secondly, the grain motion strongly affects the nucleation localization and intensity. Without grain motion, nucleation occurs in the whole ingot thickness, and starts all along the liquidus line. The undercooling only slightly increases from the centre to the surface of the ingot (Figure 5-a), and the nucleation rate increases accordingly (from 10^6 $m^{-3}.s^{-1}$ at the centre to 1.510^8 $m^{-3}.s^{-1}$ at the surface) as shown in Figure 5-b. When grain motion is added, grains continuously leave the nucleation zone (close to the surface) after being formed, maintaining a high undercooling in this zone (>1°C compared to 0,35°C in Case 1, as shown in Figure 5-a). Thus more inoculant particles can be activated. On the opposite, grains are continuously brought in the ingot centre, reducing the undercooling (<0.1°C) enough to prevent any nucleation in this area.

As the packing fraction of the grains is not known a priori, three values of packing fractions were tested, from 0.3 to 0.5, but we noticed that this parameter has a very weak influence on the grain size prediction. Thus the grain motion tends to refine and to homogenize the microstructure, and the predicted average final grain size is close to the one observed experimentally. However, the grain size

variations along the ingot thickness observed experimentally are not found by the model, which can be the sign of a missing physical phenomenon in the model. Notably, in our model the packing is described by a criterion on the local grain fraction. In the regions where the packing front is inclined the blocking of the grains is certainly not well described by such a simple criterion.

4.3. Impact of grain morphology

In the cases presented until now, grains were supposed to be globular, which was supported by experimental observations of the final grain morphology. However, this observation cannot give information about the morphology of the grains during their growth. The morphology is known to impact the growth velocity and thus the coupling between nucleation and growth. Moreover, the transport of the grains is affected by the shape of the grains. This is why we study in Case 3 the effect of grain morphology through a paraboloidal tip model.

We observe that when the grain morphology is taken into account (Case 3), the grain size profile is hardly changed compared to Case 2 where grains are supposed to be globular (Figure 4). Indeed, even if the morphology is dendritic at first in Case 3, the grains globularize before reaching the packing fraction. This can be seen in Figure 7-a where the map of internal solid fraction $g_i=g_s/g_{env}$ is shown for Case 3. More precisely, the dendritisation favors solidification in the nucleation zone, but it also amplifies the grains sedimentation. In our case, these two phenomena compensate and the equilibrium between nucleation and growth of the grains in the nucleation zone is hardly changed so the finale grain size is only slightly changed.

4.4. Impact of the grain refiner level

The nucleation model we use is adapted to inoculated castings, as the nucleation law directly depends on the size distribution of the refiner particles. Thus in order to model the non-refined case, we propose to adapt this size distribution in order to fit the final average grain size obtained experimentally. An average final grain size that is two times larger corresponds to a 8 times smaller grain density, therefore the density of each inoculant class is divided by 8 in Case 4.

As expected, the grain morphology is more dendritic in the mushy zone in Case 4 compared to Case 3, as can be seen in Figure 7. The grain dendritisation does not directly impact the packing in the nucleation zone since the morphology remains globular at the packing fraction in both cases. However, the nucleation law change highly impacts the nucleation-growth coupling in this zone. The inoculant-particle density being smaller in Case 4, the undercooling becomes higher in order to activate nuclei classes with a higher critical undercooling (Figure 6). However, this increase of undercooling is not high enough to reach the same nucleation rate as in Case 3 (Figure 8). The density of formed grains is reduced, which is the expected effect when the refiner level is reduced. This can be seen in Figure 9, where the grain diameter profile is given in Case 3 and Case 4, and is compared to the experimental profiles obtained respectively for the refined and the non-refined cases.

By reducing the refiner level, the predicted average final grain size estimation fits the non-refined case measurement. This result was not obvious because the reduction of the global nuclei population could affect the nucleation-growth competition in a nonlinear way. Thus the model not only enables to predict the average grain size without any adjustment in the refined case, but by adjusting the refiner level, it enables to predict the final grain size in the non-refined case. However, the size variations along the ingot thickness observed experimentally are not correctly predicted. Moreover, although the model predicts a globular morphology in the center of the ingot for both Case 3 and Case 4, it is more difficult to characterize the microstructure close to the surface. The reason is that the grains globularize extremely rapidly around the packing fraction (from a very dendritic to a globular morphology in 5 mm, in the sub-surface region). Although the fully dendritic morphology observed experimentally in the non-refined case is not predicted by the model, the maps in Figure 7 show a more dendritic morphology around the packing fraction close to the surface in Case 4 compared to Case 3. Thus the influence of grain refinement on the grain morphology is qualitatively well captured.

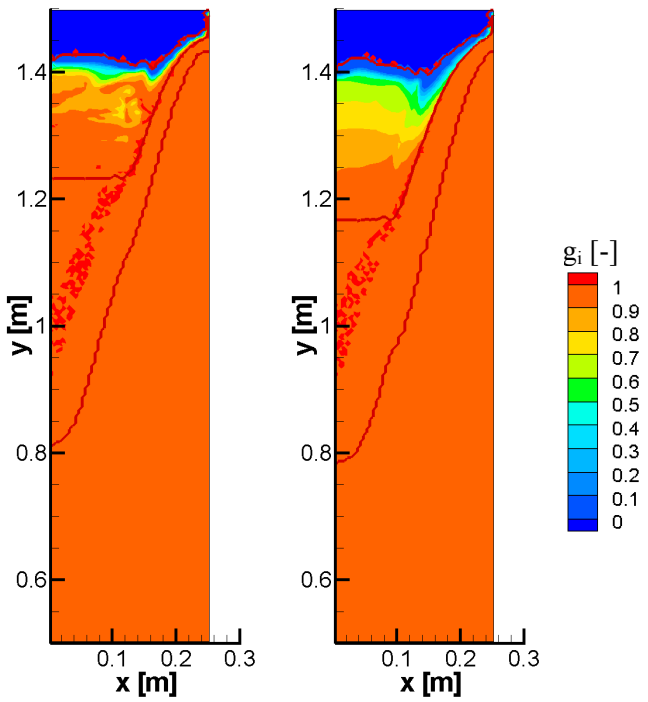

(a) Case 3 (b) Case 4

Figure 7. Internal fraction map in the mushy zone and liquidus, packing and solidus lines in red for (a) Case 3 and (b) Case 4.

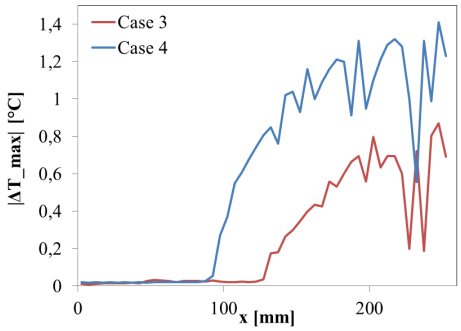

Figure 6. Maximal undercooling profiles, for Case 3 and Case 4.

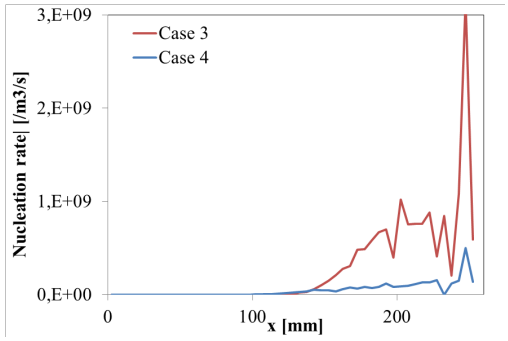

Figure 8. Nucleation rate profiles along the ingot thickness, for Case 3 and Case 4.

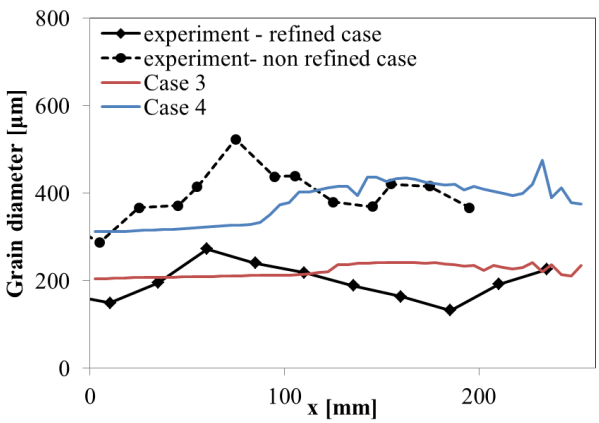

Figure 9. Grain diameter profile for Case 3 and Case 4 compared to the experimental profiles, respectively with and without refiner.

5. Summary and conclusions

The microstructure formation has been studied in a 5182-alloy industrial-scale slab of 510 mm thickness, cast without grain refiner or inoculated with 1 kg/t of Al-3Ti-1B, for which experimental grain size measurements were available. With the presented model we were able to study for the first time the coupling between nucleation and growth of the grains in presence of liquid convection and

grains and inoculant particles transport at the macroscopic scale. The comparison between the experimental grain size profile and the model results enables us to analyze the impact of each phenomenon on the grain formation.

The flow induced by natural convection and solidification shrinkage slightly amplifies the grain size heterogeneities. On the contrary, grain motion reduces them and highly reduces the average grain size. We show that grain motion is a key phenomenon for the understanding of the final microstructure size. A correct modeling of these phenomena enables us to predict an average final grain size close to the experimental observations. However, the grain size evolution across the ingot thickness is not accurately predicted. To model the non-grain-refined casting, which can present dendritic grains, we further investigated the influence of the description of grain morphology on the model prediction. The same conclusions than for the inoculated ingot can be drawn: the average grain size can be predicted but not the observed variations of the grain size across the ingot thickness.

We demonstrated that our model can predict the average final grain size in an industrial size casting. A detailed modelling of both microscopic phenomena of nucleation and growth of grains and of macroscopic phenomena of convection and grains and inoculant particles was required for that. Moreover, we could show that the influence of the grain-refiner level can be reproduced. However, further phenomena should be considered to explain the grain size distribution in the ingot. Principally, further work on the description of grain packing, a fundamental phenomenon in the transport of equiaxed grains, is required.

References

[1] Nadella R, Eskin D G and Katgerman L 2008 *Metall. Mater. Trans.* A **39** 450–61
[2] Joly A, Grün G-U, Daloz D, Combeau H and Lesoult G 2000 *Mater. Sci. Forum* **329-330** 111–20
[3] Tronche A 2000 (PhD thesis, University of Cambridge, UK)
[4] Greer A L, Bunn A M, Tronche A, Evans P V and Bristow D J 2000 *Acta Mater.* **48** 2823–35
[5] Jalanti T 2000 (PhD thesis)
[6] Vreeman C J, Schloz J D and Krane M J M 2002 J *Heat Transfer* **124** 947-53
[7] Håkonsen A, Mortensen D, Benum S and Vatne H E 1999 *Light Metals* ed Eckert C E (Warrendale, USA: TMS) pp 821–7
[8] Založnik M and Combeau H 2010 *Comput. Mater. Sci.* **48** 1–10
[9] Heyvaert L, Bedel M, Založnik M and Combeau H 2014 *International Conference on Advances in Solidification Processes 4*, Old Windsor, 8-11 June 2014
[10] Bedel M, Založnik M, Kumar A, Combeau H, Jarry P and Waz E 2012 *IOP Conf. Ser. Mater. Sci. Eng.* **27** 012070
[11] Bedel M 2014 (PhD thesis, Université de Lorraine, France)
[12] Nielsen Ø, Mo A, Appolaire B and Combeau H 2001 *Metall. Mater. Trans.* A **32** 2049–60
[13] Lesoult G, Albert V, Appolaire B, Combeau H, Daloz D, Joly A, Stomp C, Grün G-U and Jarry P 2001 *Sci. Technol. Adv. Mater.* **2** 285–91
[14] Daloz D, Combeau H, Joly A, Lesoult G, Grün G-U, Jarry P and Commet B 2002 Materiaux 2002 (Tours, France)
[15] Drezet J-M, Rappaz M, Grün G-U and Gremaud M 2000 *Metall. Mater. Trans.* A **31** 1627–34
[16] Combeau H, Založnik M, Hans S and Richy P E 2009 *Metall. Mater. Trans.* B **40** 289-304